

# Crystal Structure of Magnetolectric $\text{Ba}_2\text{MnGe}_2\text{O}_7$ at Room and Low Temperatures by Neutron Diffraction

Andrew Sazonov,<sup>\*,†,‡</sup> Vladimir Hutanu,<sup>\*,†,‡</sup> Martin Meven,<sup>†,‡</sup> Georg Roth,<sup>‡</sup> Robert Georgii,<sup>¶</sup> Takatsugu Masuda,<sup>§</sup> and Bálint Náfrádi<sup>||</sup>

<sup>†</sup>Institute of Crystallography, RWTH Aachen University and Jülich Centre for Neutron Science (JCNS) at Heinz Maier-Leibnitz Zentrum (MLZ), 85748 Garching, Germany

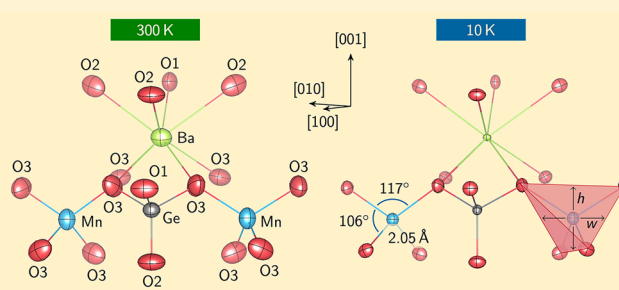
<sup>‡</sup>Institute of Crystallography, RWTH Aachen University, 52056 Aachen, Germany

<sup>¶</sup>Heinz Maier-Leibnitz Zentrum (MLZ) and Physics Department E21, Technical University of Munich, 85748 Garching, Germany

<sup>§</sup>International Graduate School of Arts and Sciences, Yokohama City University, Yokohama, Kanagawa 236-0027, Japan

<sup>||</sup>École Polytechnique Fédérale de Lausanne, Laboratory of Nanostructures and Novel Electronic Materials, 1015 Lausanne, Switzerland

**ABSTRACT:** For a symmetry-consistent theoretical description of the ferroelectric phase of  $\text{Ba}_2\text{MnGe}_2\text{O}_7$  melilite compound, a precise knowledge of its crystal structure is a prerequisite. Here we report results of single-crystal neutron diffraction experiments on  $\text{Ba}_2\text{MnGe}_2\text{O}_7$  at room (300 K) and low (10 K) temperatures. The structural model based on the tetragonal space group  $P\bar{4}2_1m$  describes the  $\text{Ba}_2\text{MnGe}_2\text{O}_7$  symmetry both at room and low temperatures. We found reflections forbidden in the typical  $P\bar{4}2_1m$  melilite-type structure. A comparison of the experimental data collected by means of both thermal and cold neutrons with simulated multiple diffraction patterns allows us to unambiguously demonstrate that forbidden peaks originate from multiple diffraction (Renninger effect) rather than from real symmetry lowering. The precise structural parameters at 300 and 10 K are presented for the first time and compared with those of other magnetolectric melilite-type germanates.



## INTRODUCTION

Recently, electric polarization under applied magnetic field has been reported for different barium-based melilite-type germanates  $\text{Ba}_2\text{XGe}_2\text{O}_7$  ( $X = \text{Mn}, \text{Co}, \text{Cu}$ ).<sup>1</sup> Neither the generally accepted spin-current, nor exchange-striction models of multiferroicity are applicable in these materials, and a novel spin-dependent p–d hybridization mechanism was proposed to describe their magnetolectric behavior independent of the type of the magnetic ions.<sup>1</sup> Within this model, the oxygen coordination of the magnetic ion in the  $\text{XO}_4$  tetrahedron plays an important role. The resulting electric polarization is determined by the lengths of the X–O chemical bonds and the rotation angle of the whole  $\text{XO}_4$  tetrahedron to the [110] axis. It was postulated that all the above-mentioned compounds are isostructural having the typical melilite symmetry with tetragonal space group (SG)  $P\bar{4}2_1m$  in analogy to the structure of Co-åkermanite  $\text{Ca}_2\text{CoSi}_2\text{O}_7$  published in 1993.<sup>2</sup> For instance, in order to perform density functional theory calculations and model cluster Hamiltonian analysis in the theoretical investigation of  $\text{Ba}_2\text{CoGe}_2\text{O}_7$ , the Ca ions were simply substituted by Ba and Si by Ge for the qualitative description of the observed magnetolectric behavior in this compound.

In general, the members of the melilite group are known to show a variety of structural phase transitions. For example, a recent detailed study on  $\text{Ca}_2\text{CoSi}_2\text{O}_7$ <sup>3,4</sup> shows that it has the tetragonal SG  $P\bar{4}2_1m$  only at high temperatures. At about 500 K its crystal structure changes from the high-temperature state with tetragonal SG  $P\bar{4}2_1m$  and lattice parameters  $a = b \approx 7.86 \text{ \AA}$  and  $c \approx 5.03 \text{ \AA}$  to an incommensurately modulated phase with two propagation vectors.<sup>3,4,6</sup> Below 270–160 K, a commensurately modulated lock-in structure stabilizes with a  $(3 \times 3 \times 1)$  supercell and lattice parameters  $a \approx b \approx 23.51 \text{ \AA}$  and  $c \approx 5.03 \text{ \AA}$  in the orthorhombic SG  $P2_12_12_1$ .<sup>3,7</sup> In this superstructure,  $\text{CoO}_4$  tetrahedra are distorted and rotated to different degrees. The deformation of the high-temperature structure and the corresponding symmetry changes are related to a misfit between the layers formed by  $\text{CoO}_4$  and  $\text{Si}_2\text{O}_7$  groups and interlayer Ca cations.<sup>4,8</sup>

Recently, another mechanism of multiferroicity in barium-based melilite-type germanates  $\text{Ba}_2\text{XGe}_2\text{O}_7$  ( $X = \text{Ni}, \text{V}$ ) has been proposed, considering Jahn–Teller (JT) distortion as a main source for the electric polarization.<sup>9</sup> Within this model, the precise structural information on the  $\text{XO}_4$  tetrahedrons also

Received: January 17, 2018

Published: April 9, 2018

plays an important role. Again, because of the lack of the experimental data, the authors in their theoretical work used  $\text{Ba}_2\text{CoGe}_2\text{O}_7$  structural parameters from ref 10 and substituted Co by Ni, which is Jahn–Teller active. This mechanism can be applicable to  $\text{Ba}_2\text{MnGe}_2\text{O}_7$  indicating the difference compared to  $\text{Ba}_2\text{CoGe}_2\text{O}_7$ . Therefore, the distortion of the magnetic cation tetrahedron is an essential information to check the validity of this mechanism. JT distortion is known to play a role also in  $\text{Ba}_2\text{CuGe}_2\text{O}_7$ , where the  $\text{CuO}_4$  tetrahedra are significantly deformed along the  $c$  axis.<sup>11</sup> Little is known, however, how this distortion develops with temperature and whether germanates show similar to  $\text{Ca}_2\text{CoSi}_2\text{O}_7$  symmetry reduction, especially at temperatures where the magnetic ordering and magnetoelectricity occur.

Moreover, the type of magnetic ion in these melilites plays a key role in the established magnetic order and as a result in the spin-induced polarization. Indeed,  $\text{Ba}_2\text{CuGe}_2\text{O}_7$  ( $S = 1/2$ ) orders into a cycloidal spin modulated structure with a magnetic propagation vector  $k = (1 + \xi, \pm \xi, 0)$ , with  $\xi = 0.027$  below 3.2 K.<sup>12</sup>  $\text{Ba}_2\text{CoGe}_2\text{O}_7$  ( $S = 3/2$ ) has a 2D-like magnetic structure with zero propagation vector  $k = 0$ . It is characterized by collinear antiferromagnetic (AFM) order in the  $ab$  plane and ferromagnetic (FM) coupling along the  $c$  axis.<sup>13</sup>  $\text{Ba}_2\text{MnGe}_2\text{O}_7$  ( $S = 5/2$ ) also has AFM spin arrangement in the  $ab$  plane, but the coupling between the layers along  $c$  is AFM<sup>1,14</sup> and the propagation vector is  $k = (0,0,1/2)$ . Note that the magnetoelectric coupling strength in  $\text{Ba}_2\text{MnGe}_2\text{O}_7$  in the paramagnetic state at 50 K is about 2 orders of magnitude lower compared to that in  $\text{Ba}_2\text{CuGe}_2\text{O}_7$  or  $\text{Ba}_2\text{CoGe}_2\text{O}_7$  (ref 1.) despite  $\text{Mn}^{2+}$  having the largest value of the magnetic moment in this family of compounds. The canting of the magnetic moments in the  $ab$  plane (weak ferromagnetism) was suggested to lead to electric polarization in  $\text{Ba}_2\text{CoGe}_2\text{O}_7$ .<sup>15</sup> No such ferromagnetic component has been reported for  $\text{Ba}_2\text{MnGe}_2\text{O}_7$  so far.

Considering that magnetic symmetry is generally related to the nuclear one by a group–subgroup relation it is an additional argument suggesting that not all the barium-based melilite-type germanates must be strictly isostructural at low temperatures. The knowledge about their precise crystal structures is therefore a very important prerequisite to understand magnetoelectric phenomena generally in multiferroics and particularly in melilites. For instance, in the work of ref 15, the main features of the magnetoelectric behavior of, for instance,  $\text{Ba}_2\text{CoGe}_2\text{O}_7$  were predicted by symmetry considerations only, without referring to any specific microscopic mechanism. Thus, the exact structural model including, of course, the true symmetry is often an essential starting point for further theoretical and experimental research. However, the crystal structure of  $\text{Ba}_2\text{MnGe}_2\text{O}_7$  at low temperature was not studied up to now. Moreover, detailed structural information, e.g., atomic coordinates and displacement parameters are not published even for room temperature structure. The only available structural information is given by refs 1 and 14 and limited to the lattice parameters only, determined at room temperature with a laboratory X-ray powder diffractometer. We should note here, that very accurate measurements are required in order to determine the true symmetry and to exclude parasitic effects, such as multiple diffraction, higher order wavelength contamination, etc. Quite a number of examples show<sup>7,8,10,16</sup> how important it is not to draw wrong conclusions about the crystal symmetry of the studied melilites from observed reflections violating the systematic extinction rule.

Multiple diffraction quite often manifests itself in the X-ray and neutron diffraction experiment for large and perfect crystals (as in our case), but this effect is rarely taken into account. The absence of absorption for most elements/isotopes also increases the probability for multiple diffraction.

To fill the gap of crystal structure information on  $\text{Ba}_2\text{MnGe}_2\text{O}_7$  and to provide accurate and reliable data for further experimental and theoretical research, we performed single-crystal neutron diffraction experiments at room (300 K) and low (10 K) temperatures. Both short (thermal neutrons) and long (cold neutrons) wavelengths were applied in order to differentiate between real symmetry lowering and multiple diffraction (Renninger effect) (see, e.g., refs 17 and 18 and references therein). At room temperature, we are not affected by the limitations in the sample rotation due to the cryostat. This allowed us to determine the origin of reflections on the forbidden positions in the same experimental conditions as full data collection for the structure refinement. The low temperature is chosen in order to check if there are any structural changes down to the temperatures close to the magnetic phase transition (4 K). The precise structural studies in the magnetic phase are usually complicated due to the additional magnetic contribution to the Bragg reflections and the results are not always unambiguous: Weak distortion is often hidden and not detectable. Measurements just above the magnetic phase transition provide the reliable information about the crystal structure in the parent paramagnetic phase and may serve as an essential base for the future magnetic symmetry analysis. The obtained precise structural parameters of  $\text{Ba}_2\text{MnGe}_2\text{O}_7$  are compared with literature data on other barium germanates with different magnetic ions.

## ■ EXPERIMENTAL SECTION

Single crystals of  $\text{Ba}_2\text{MnGe}_2\text{O}_7$  were grown by floating-zone technique and characterized in previous studies.<sup>14</sup> The sample used for the neutron diffraction experiment has a cylindrical shape of approximately 6 mm in height and about the same diameter.

Single-crystal neutron diffraction studies with both short and long wavelengths were performed on two diffractometers, HEiDi<sup>19</sup> and MIRA,<sup>20,21</sup> at the research neutron source FRM II at the Heinz Maier-Leibnitz Zentrum (MLZ), Germany.

The full data collections for the structural refinement were done on HEiDi both at 300 K with the wavelength  $\lambda = 0.55$  Å obtained from a Cu(420) and at 10 K with the wavelength  $\lambda = 0.79$  Å obtained from a Ge(422) monochromator. For the azimuthal ( $\psi$ ) scans on HEiDi, the largest available wavelength  $\lambda = 1.17$  Å obtained from a Ge(311) monochromator was applied. A <sup>3</sup>He point detector, optimized for neutrons with short wavelength, was used in the experiments on HEiDi.

On MIRA, the wavelength  $\lambda = 4.488$  Å was obtained from a HOPG (highly oriented pyrolytic graphite) monochromator with Be-filter to suppress the  $\lambda/2$  contamination. Both point and position sensitive detectors were used for the measurements of  $\psi$  scans at room temperature.

On both instruments, an Eulerian cradle was used and the sample was oriented in a way to have the forbidden reflections of the ( $h00$ ) type in the scattering plane when the  $\chi$  angle in the conventional 4-cycle geometry was close to 90°. This geometry allows an easy rotation around  $\psi$  by 360° as it almost coincides with the conventional  $\phi$  rotation. As the first step of the measurements, the orientation matrix was accurately refined. Second, the conventional  $\theta$ ,  $\omega$ ,  $\chi$  and  $\phi$  values for any of the requested  $\psi$  angles were calculated by the data collection program DIF4 for HEiDi. Then, an  $\omega$  scan was performed for each  $\psi$  value and the integrated intensity of the scan was assigned to that  $\psi$  point. As a result, the integrated intensity versus  $\psi$  curve was obtained

and further compared with the calculations of possible multiple diffraction.

The integrated intensities of the reflections collected with a point detector were obtained using the DAVINCI program.<sup>22</sup> The multiple diffraction patterns were simulated using the UMWEG program.<sup>23</sup> The structural parameters of Ba<sub>2</sub>MnGe<sub>2</sub>O<sub>7</sub> were refined from the full data collection using the JANA2006 program.<sup>24</sup> Experimental and refinement details are summarized in Table 1.

**Table 1. Single-Crystal Neutron Diffraction Experimental and Refinement Details**

	Crystal Data	
chemical formula	Ba <sub>2</sub> MnGe <sub>2</sub> O <sub>7</sub>	Ba <sub>2</sub> MnGe <sub>2</sub> O <sub>7</sub>
<i>M<sub>r</sub></i>	586.8	586.8
cell setting, space group	tetragonal, <i>P</i> 4̄2 <sub>1</sub> <i>m</i>	tetragonal, <i>P</i> 4̄2 <sub>1</sub> <i>m</i>
<i>T</i> (K)	300	10
<i>a</i> , <i>c</i> (Å)	8.509(2), 5.529(5)	8.498(2), 5.512(5)
<i>V</i> (Å <sup>3</sup> )	400.3(4)	398.1(4)
<i>Z</i>	2	2
<i>D<sub>x</sub></i> (Mg m <sup>-3</sup> )	4.896	4.896
radiation type	constant wavelength neutron	constant wavelength neutron
	diffraction, $\lambda = 0.55 \text{ \AA}$	diffraction, $\lambda = 0.79 \text{ \AA}$
$\mu$ (mm <sup>-1</sup> )	0.003	0.003
crystal form, color	cylinder, dark blue	cylinder, dark blue
crystal size (mm)	6 × 3 (radius)	6 × 3 (radius)
	Data Collection	
diffractometer	four-circle diffractometer	four-circle diffractometer
radiation source	nuclear reactor	nuclear reactor
monochromator	Cu(420)	Ge(422)
<i>T</i> (K)	300	10
data collection method	$\omega$ scans	$\omega$ scans
$[\sin \theta/\lambda]_{\max}$ (Å <sup>-1</sup> )	1.04	0.81
range of <i>h</i> , <i>k</i> , <i>l</i>	-13 → <i>h</i> → 11 -15 → <i>k</i> → 0 -11 → <i>l</i> → 5	0 → <i>h</i> → 12 -13 → <i>k</i> → 13 -8 → <i>l</i> → 8
no. of measured reflections	3464	1663
no. of independent reflections	1524	964
no. of independent reflections with <i>I</i> > 3σ( <i>I</i> )	1465	962
<i>R</i> <sub>int</sub>	0.032	0.023
	Refinement	
refinement on	<i>F</i>	<i>F</i>
<i>R</i> [ <i>F</i> > 3σ( <i>F</i> )], <i>wR</i> ( <i>F</i> ), <i>S</i>	0.028, 0.043, 1.73	0.025, 0.034, 3.99
no. of reflections	1465	962
no. of parameters	35	35
weighting scheme, <i>w</i>	1/[σ <sup>2</sup> ( <i>F</i> ) + 0.0001 <i>F</i> <sup>2</sup> ]	1/[σ <sup>2</sup> ( <i>F</i> ) + 0.0001 <i>F</i> <sup>2</sup> ]
extinction correction	isotropic	isotropic
	Lorentzian type 1 <sup>a</sup>	Lorentzian type 1 <sup>a</sup>
extinction coefficient	0.017(8)	0.048(9)

<sup>a</sup>According to ref 25.

## RESULTS AND DISCUSSION

**Origin of Forbidden Reflections.** In both single-crystal X-ray and neutron diffraction studies performed with short wavelengths ( $\lambda \lesssim 1.2 \text{ \AA}$ ) on melilite compounds, weak intensities at the positions of reflections violating the systematic extinctions for the 2<sub>1</sub> symmetry element and thus forbidden in the tetragonal SG *P*4̄2<sub>1</sub>*m*, such as, e.g., (*h*00), with *h* = 2*n* + 1

and *n* ∈  $\mathbb{Z}$  are often observed.<sup>8,10,16</sup> Such reflections up to high order were observed in the studied Ba<sub>2</sub>MnGe<sub>2</sub>O<sub>7</sub> single crystal at different diffractometers, with various wavelengths and at several temperatures (down to 10 K). The intensities of those reflections are usually larger than three times their standard deviations (3σ) despite the fact that they are relatively weak compared to the allowed main peaks. In most cases, such forbidden reflections can be explained by magnetic contributions, higher order wavelength contamination, multiple diffraction or symmetry lowering. In a strict sense any violation of the systematic extinction rule mentioned above even by a single reflection is already sufficient to question the considered space group. Therefore, the origin of observed forbidden reflections in Ba<sub>2</sub>MnGe<sub>2</sub>O<sub>7</sub> should be carefully verified in order to avoid incorrect conclusions about its true crystal structure. Figure 1 shows the comparison of peak profiles for an allowed reflection (330) with those for the forbidden peaks (300) and (500) collected with the wavelength  $\lambda = 1.17 \text{ \AA}$ , as an example. The widths of the observed peaks are comparable and limited by the instrumental resolution and sample mosaicity.

We briefly go through the above-mentioned possible reasons for observing forbidden reflection. First, the long-range magnetic order in Ba<sub>2</sub>MnGe<sub>2</sub>O<sub>7</sub> develops far below room temperature, at *T<sub>N</sub>* ≈ 4K.<sup>1,14</sup> Thus, the magnetic contribution unambiguously cannot be origin of the observed intensities.

Second, in the case of the Ge(311) monochromator with  $\lambda = 1.17 \text{ \AA}$ ,  $\lambda/2$  contribution is fully suppressed due to the extinction rule of the SG and  $\lambda/3$  is expected to be less than 0.4% of the intensity of the first order diffraction peak. Moreover, all tripled reflection indices (3*h*,0,0), with *h* = 2*n* + 1 and *n* ∈  $\mathbb{Z}$  are forbidden in the tetragonal space group *P*4̄2<sub>1</sub>*m* and thus the third order contribution is ruled out. Therefore, higher-order wavelength contamination can also be excluded from the possible set of explanations of the observed reflections.

Finally, additional experiments were performed in order to choose between real symmetry lowering and multiple diffraction. Prior to the experiments, a possible multiple diffraction contribution was estimated by simulation of the azimuthal ( $\psi$ ) scans. The instrumental parameters used in the simulation are the horizontal and vertical beam divergences ( $\delta_H$ ,  $\delta_V$ ) and wavelength spread ( $\Delta\lambda/\lambda$ ) of the incident beam. Those were selected based on the geometry of the instrument. The Ba<sub>2</sub>MnGe<sub>2</sub>O<sub>7</sub> sample specific parameters, like mosaic spread ( $\nu$ ) and mosaic-block radius (*r*) were set manually. Fractional atomic coordinates (*x*, *y*, *z*) and anisotropic atomic displacement parameters (ADPs, *U*<sub>aniso</sub>) for Ba<sub>2</sub>MnGe<sub>2</sub>O<sub>7</sub> were obtained from structure refinement using the present single-crystal neutron diffraction data (see next section).

Figure 2 (left and middle panels) shows the comparison of the simulated multiple diffraction pattern for two forbidden (300) and (500) reflections and the experimental data collected at the HEiDi diffractometer with  $\lambda = 1.17 \text{ \AA}$ . The following parameters were used in the calculations:  $\Delta\lambda/\lambda = 0.01$ ,  $\delta_H = 1.6^\circ$ ,  $\delta_V = 1.6^\circ$ , *r* = 400 μm, and  $\nu = 1.5^\circ$ . A good agreement between the calculated and experimental data indicates that both instrumental and sample specific parameters were reasonably selected. As can be seen from the left and middle panels of Figure 2, there is no single point in the diffraction pattern without any overlap of the neighboring reflections and the intensity never drops down to zero. The very broad peaks on the  $\psi$  scan make it almost impossible to separate the case of symmetry lowering from that of multiple diffraction because a

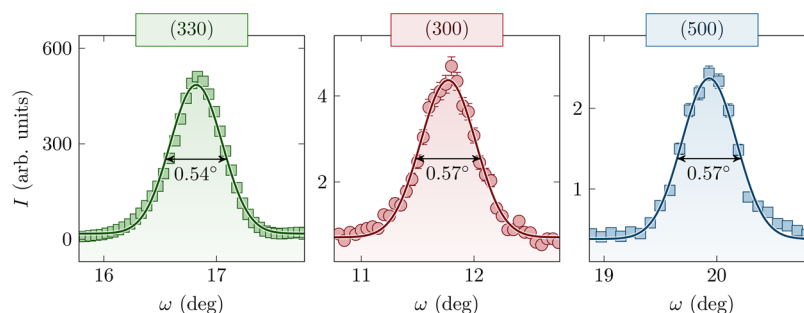


**Figure 1.** Comparison of allowed (330) and forbidden (300) and (500) peak profiles indicating comparable peak widths of the reflections. Data were collected at 300 K with  $\lambda = 1.17$  Å. The solid line is a Gaussian fit. Full widths at half-maximum are indicated. Error bars are smaller than the symbol size if not given.

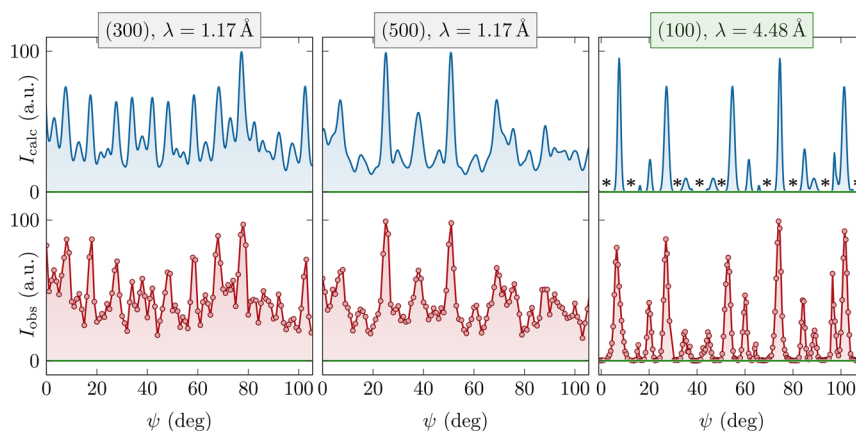


**Figure 2.** Multiple diffraction patterns of forbidden (300), (500), and (100) reflections of  $\text{Ba}_2\text{MnGe}_2\text{O}_7$  according to calculations (top blue curves) and single-crystal neutron diffraction experiments (bottom red curves) with short ( $\lambda = 1.17$  Å) and long ( $\lambda = 4.49$  Å) wavelengths. Star symbols indicate regions of zero intensity in the  $\psi$  scans with long wavelength confirming a multiple diffraction origin of the observed forbidden reflections in  $\text{Ba}_2\text{MnGe}_2\text{O}_7$ .

possible contribution caused by symmetry reduction could be hidden by the multiple diffraction part.

In contrast to the short wavelength case, cold neutrons allow us to overcome the problem with overlapping peaks in the  $\psi$  scans. A change of just one single parameter, the wavelength  $\lambda$ , in the simulation process from  $\lambda = 1.17$  Å to  $\lambda = 4.49$  Å drastically modifies the entire multiple diffraction pattern. The number of  $\psi$  peaks is reduced and they become well separated from each other: Regions of zero intensity appear on the simulated curve (marked by the star symbols in Figure 2, right panel). The experimental multiple diffraction pattern using long neutron wavelength is shown in the bottom right panel of Figure 2. An adjustment of the instrumental parameters allows us to achieve a better agreement between experimental data and calculations. In the simulations with cold neutrons, the following parameters were used:  $\Delta\lambda/\lambda = 0.01$ ,  $\delta_{\text{H}} = 0.5^\circ$ ,  $\delta_{\text{V}} = 0.5^\circ$ ,  $r = 400$   $\mu\text{m}$ , and  $\nu = 1.5^\circ$ . Note that the instrument related parameters correspond to the typical values of the MIRA diffractometer and the sample specific parameters are the same as given above in the simulation with short wavelength. In this experiment, we selected the forbidden (100) reflection for measurement because (300) or (500) reflections were not accessible with the long wavelength. The experimental values for (100) agree well with the calculation as can be seen in Figure 2 (right panel). We were able to successfully reproduce the zero-intensity regions experimentally. Therefore, the observed intensity on the positions of forbidden reflections could be explained solely by multiple diffraction without

referring to any additional contribution. This supports the tetragonal SG  $P\bar{4}2_1m$  to be the correct description of the true structure of  $\text{Ba}_2\text{MnGe}_2\text{O}_7$  at room temperature, similar to the case of  $\text{Ba}_2\text{CoGe}_2\text{O}_7$ .<sup>16</sup>

The limitations caused by the necessity of using a cryostat did not allow us to perform low temperature  $\psi$  scans on MIRA. Nevertheless, we believe that the origin of the forbidden reflections at 10 K (slightly above  $T_{\text{N}} \approx 4$  K) is also governed by multiple diffraction, because their absolute and relative intensities are found to be similar to those measured at room temperature.

**Structural Details at Room and Low Temperatures.** In order to determine the precise structural parameters for  $\text{Ba}_2\text{MnGe}_2\text{O}_7$  at room (300 K) and low (10 K) temperatures we performed a refinement from our neutron diffraction data using the typical melilite crystal structure model with SG  $P\bar{4}2_1m$  confirmed in the previous section. The starting parameters were taken from the isostructural compound  $\text{Ba}_2\text{CoGe}_2\text{O}_7$ , the structure of which was precisely determined by neutron diffraction.<sup>16,26</sup> All atomic positions that are not restricted by symmetry were refined together with anisotropic atomic displacements ( $U_{\text{aniso}}$ ), scale, and extinction parameters. At the final stage, the refinement was done varying also the occupancies of the Mn, Ge, and O sites. Those parameters are found to be 0.97(1)–0.98(1), which deviate only marginally from the ideal value of 1. It should be noted here that multiple diffraction redistributes the intensities between strong and weak reflections, but the effect is, on the average, not very large and

cannot be corrected for in a phenomenological way (as for extinction). Therefore, the experimentally determined intensities of the main Bragg reflections (without corrections for Renninger effect) were used in the refinement.

A very good agreement between the experimental and calculated data for both 300 and 10 K (see Figure 3) confirms

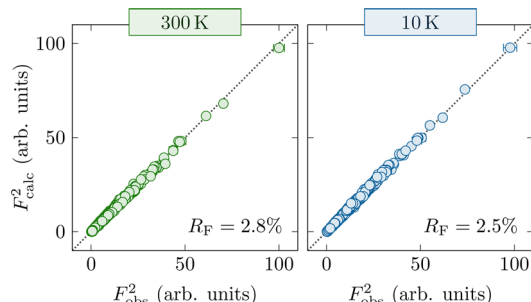


**Figure 3.** Quality of the  $\text{Ba}_2\text{MnGe}_2\text{O}_7$  crystal structure refinement in SG  $P4_21m$  according to presented single-crystal neutron diffraction data at 300 and 10 K. Experimentally measured integrated intensities ( $F_{\text{obs}}^2$ ) are plotted against the calculated ones ( $F_{\text{calc}}^2$ ). Reliability factors  $R_F$  are given.

the correctness of the selected crystal structure model. Table 2 presents the refined atomic coordinates as well as the isotropic atomic displacement ( $U_{\text{iso}}$ ) parameters, while  $U_{\text{aniso}}$  are given in Table 3. Full details of the refinement, including bond lengths and angles, are deposited in the crystallographic information file (CIF). Figure 4 shows a fragment of  $\text{Ba}_2\text{MnGe}_2\text{O}_7$  crystal structure with the atomic bonds for both room (300 K, left panel) and low (10 K, right panel) temperatures.

In this structure,  $\text{Mn}^{2+}$  forms flattened  $\text{MnO}_4$  tetrahedra with Mn–O bond length of 2.0491(3) Å at room temperature. This value is found to be larger compared to 1.9824(4) Å and 1.95(1) Å for Co–O in  $\text{Ba}_2\text{CoGe}_2\text{O}_7$ <sup>16</sup> and Cu–O in  $\text{Ba}_2\text{CuGe}_2\text{O}_7$ ,<sup>11</sup> respectively. The differences between those bond lengths compares well with the differences in the ionic radii of Mn, Co and Cu.<sup>27</sup> The O–Mn–O angles of 105.86(2) and 116.96(2)° indicate a compression of the tetrahedra along the tetragonal  $c$  axis (Figure 4). If the height of the tetrahedron is called  $h$  and its width  $w$ , as denoted in Figure 4, then the ratio  $h/w$  indicates a degree of compression. For  $\text{Ba}_2\text{MnGe}_2\text{O}_7$ , this ratio is found to be about 0.87, i.e., the tetrahedra are

compressed by 13% compared to the regular ones with  $h/w = 1$ . Note that the long axis of the Mn displacement ellipsoids is also aligned along the  $c$  axis; the anisotropy is small, but clearly visible (Figure 4). The same degree of tetrahedral compression (13%) is also found in  $\text{Ba}_2\text{CoGe}_2\text{O}_7$ .<sup>16</sup> In contrast,  $\text{Ba}_2\text{CuGe}_2\text{O}_7$  is characterized by a significantly stronger compression of about 24%.<sup>11</sup> The large distortion of the  $\text{CuO}_4$  tetrahedra is most probably associated with the Jahn–Teller active ion  $\text{Cu}^{2+}$ .

$\text{Ba}^{2+}$  occupies an eight-coordinated site and the distances between the Ba and O atoms are in the range 2.7119(5)–2.9746(6) Å. The average  $\langle\text{Ba–O}\rangle$  length is 2.836 Å, a value close to the value of 2.824 Å reported for  $\text{Ba}_2\text{CoGe}_2\text{O}_7$ , but it is shorter than the value of 2.879 Å in  $\text{Ba}_2\text{CuGe}_2\text{O}_7$ . Ge–O distances of tetrahedral  $\text{Ge}^{4+}$  range between 1.7223(5) Å and 1.7925(3) Å, with an average of 1.756 Å. This value is very similar to 1.758 Å in  $\text{Ba}_2\text{CoGe}_2\text{O}_7$ , but again smaller compared to 1.782 Å in  $\text{Ba}_2\text{CuGe}_2\text{O}_7$ . As can be seen in Figure 4, the displacement ellipsoids of both Ba and Ge atoms are close to spheres, whereas those of O are clearly anisotropic with their long axis lying close to the  $ab$  plane.

A comparison of the room-temperature structure of  $\text{Ba}_2\text{MnGe}_2\text{O}_7$  with the low temperature one shows a negligible difference in the positional parameters. The most evident deviations appear for the oxygen atoms, as to be expected. The largest change of atomic coordinates of approximately 0.009 Å is found for O2, with the main shift along the  $z$  axis; The average change calculated for all the atoms is approximately 0.005 Å. The Mn–O bond length decreases from of 2.0491(3) Å at 300 K to 2.0458(7) Å at 10 K. The main change in structural parameters is found for the atomic displacements. Figure 4 shows the displacement ellipsoids drawn at 99% probability level. As expected, the ADPs parameters decrease strongly with temperature lowering. The ratios of ADP ellipsoid axes found to be similar at room and low temperatures for most atoms. A slight change is found for Mn; its ellipsoid of displacement becomes more spherical with decreasing temperature (10 K).

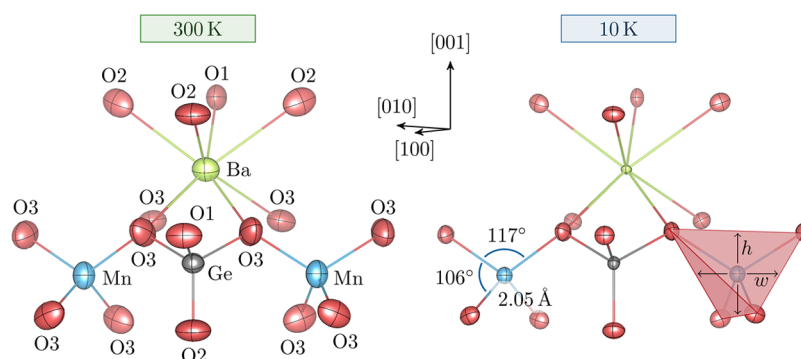
Also, both at room (300 K) and low (10 K) temperatures, the structural parameters of  $\text{Ba}_2\text{MnGe}_2\text{O}_7$  are found to be very similar to those obtained for  $\text{Ba}_2\text{CoGe}_2\text{O}_7$ .<sup>10,16</sup> At room temperature, the largest difference in the atomic positions between  $\text{Ba}_2\text{MnGe}_2\text{O}_7$  and  $\text{Ba}_2\text{CoGe}_2\text{O}_7$  is found for O2 and it

**Table 2.** Fractional Atomic Coordinates ( $x, y, z$ ) and Isotropic Atomic Displacement Parameters  $U_{\text{iso}}$  (Å<sup>2</sup>) for  $\text{Ba}_2\text{MnGe}_2\text{O}_7$  Refined in SG  $P4_21m$  According to Presented Single-Crystal Neutron Diffraction Data at 300 and 10 K

ion	Wyckoff position	$x$	$y$	$z$	$U_{\text{iso}}$
300 K					
Ba	4e	0.33456(4)	$0.5 - x$	0.49259(8)	0.00849(7)
Mn	2b	0	0	0	0.00855(12)
Ge	4e	0.13886(2)	$0.5 - x$	0.04516(4)	0.00651(4)
O1	2c	0	0.5	0.16145(11)	0.01139(9)
O2	4e	0.13858(4)	$0.5 - x$	0.73371(7)	0.01256(6)
O3	8f	0.07827(5)	0.18948(4)	0.19373(6)	0.01196(7)
10 K					
Ba	4e	0.33468(8)	$0.5 - x$	0.49290(16)	0.00154(14)
Mn	2b	0	0	0	0.00380(30)
Ge	4e	0.13904(5)	$0.5 - x$	0.04577(10)	0.00245(11)
O1	2c	0	0.5	0.16270(20)	0.00440(20)
O2	4e	0.13831(8)	$0.5 - x$	0.73300(16)	0.00528(15)
O3	8f	0.07805(9)	0.18926(9)	0.19529(12)	0.00494(15)

**Table 3.** Anisotropic Atomic Displacement Parameters  $U_{\text{aniso}}$  ( $\text{\AA}^2$ ) for  $\text{Ba}_2\text{MnGe}_2\text{O}_7$  Refined in SG  $P\bar{4}2_1m$  According to Presented Single-Crystal Neutron Diffraction Data at 300 and 10 K

ion	$U_{11}$	$U_{22}$	$U_{33}$	$U_{12}$	$U_{13}$	$U_{23}$
300 K						
Ba	0.00850(11)	$U_{11}$	0.00849(12)	0.00240(11)	-0.00086(8)	$-U_{13}$
Mn	0.00733(18)	$U_{11}$	0.01100(20)	0	0	0
Ge	0.00669(7)	$U_{11}$	0.00615(7)	0.00049(8)	0.00007(4)	$-U_{13}$
O1	0.01254(16)	$U_{11}$	0.00909(17)	0.00653(19)	0	0
O2	0.01528(11)	$U_{11}$	0.00712(11)	0.00324(16)	0.00068(8)	$-U_{13}$
O3	0.01612(14)	0.00798(12)	0.01177(10)	-0.00296(10)	-0.00224(9)	0.00092(8)
10 K						
Ba	0.00160(18)	$U_{11}$	0.00140(30)	0.00000(30)	-0.00030(20)	$-U_{13}$
Mn	0.00370(40)	$U_{11}$	0.00390(50)	0	0	0
Ge	0.00226(16)	$U_{11}$	0.00280(20)	-0.00014(20)	0.00013(12)	$-U_{13}$
O1	0.00410(20)	$U_{11}$	0.00500(40)	0.00150(40)	0	0
O2	0.00590(20)	$U_{11}$	0.00400(30)	0.00140(30)	-0.00027(18)	$-U_{13}$
O3	0.00590(30)	0.00390(30)	0.00500(20)	-0.00110(20)	-0.00045(19)	0.00034(19)

**Figure 4.** Perspective view of a fragment of the  $\text{Ba}_2\text{MnGe}_2\text{O}_7$  crystal structure at 300 and 10 K, showing atomic bonds and atom labels. Displacement ellipsoids are drawn at 99% probability level. Bond distances and angles for the  $\text{MnO}_4$  tetrahedra are given.  $h$  and  $w$  denote height and width of the tetrahedron, respectively.

is equal to approximately 0.056  $\text{\AA}$ .  $\text{Ba}_2\text{CoGe}_2\text{O}_7$  and  $\text{Ba}_2\text{CuGe}_2\text{O}_7$ , on the other hand, have much larger differences as a result of Jahn–Teller distortions associated with the  $\text{Cu}^{2+}$  ions.

## CONCLUSIONS

Detailed crystallographic studies of the magnetoelectric compound  $\text{Ba}_2\text{MnGe}_2\text{O}_7$  were performed at both room (300 K) and low (10 K) temperatures using a unique combination of the short and long wavelength single-crystal neutron diffraction techniques as well as simulations of the multiple diffraction events. The crystal structure of  $\text{Ba}_2\text{MnGe}_2\text{O}_7$  can be described by the tetragonal SG  $P\bar{4}2_1m$  without any symmetry lowering, despite the intensities observed at the positions of reflections forbidden in the tetragonal SG  $P\bar{4}2_1m$  typical for melilites. By comparison of azimuthal ( $\psi$ ) scans measured at room temperature with both thermal and cold neutrons with the calculated multiple diffraction patterns we demonstrated that the scattered intensities detected at positions of forbidden reflections are entirely due to the multiple diffraction (Renninger effect). The crystal structure of  $\text{Ba}_2\text{MnGe}_2\text{O}_7$  remains the same down to at least 10 K with negligible change of atomic coordinates compared to 300 K. Although absolute values of the ADP parameters decrease significantly at lower temperature, their anisotropy remains similar to that at room temperature. The structure of  $\text{Ba}_2\text{MnGe}_2\text{O}_7$  is compared with other barium germanates having different magnetic ions. The precise structural parameters of  $\text{Ba}_2\text{MnGe}_2\text{O}_7$  both at room and

low temperatures are reported here for the first time. Our results provide foundations for further theoretical and experimental studies of this compound and other members of the melilite group exhibiting magnetoelectric behavior.

## ASSOCIATED CONTENT

### Accession Codes

CCDC 1813227–1813228 contain the supplementary crystallographic data for this paper. These data can be obtained free of charge via [www.ccdc.cam.ac.uk/data\\_request/cif](http://www.ccdc.cam.ac.uk/data_request/cif), or by emailing [data\\_request@ccdc.cam.ac.uk](mailto:data_request@ccdc.cam.ac.uk), or by contacting The Cambridge Crystallographic Data Centre, 12 Union Road, Cambridge CB2 1EZ, UK; fax: +44 1223 336033.

## AUTHOR INFORMATION

### Corresponding Authors

\*E-mail: [mail@sazonov.org](mailto:mail@sazonov.org).

\*E-mail: [vladimir.hutanu@frm2.tum.de](mailto:vladimir.hutanu@frm2.tum.de).

### ORCID

Andrew Sazonov: 0000-0002-8916-6319

Bálint Náfrádi: 0000-0001-9543-2970

### Notes

The authors declare no competing financial interest.

## ACKNOWLEDGMENTS

This work was partly supported by BMBF under Contract 05K13PA3. Part of the work is based on experiments

performed at the HEiDi instrument operated by RWTH Aachen/FZ Jülich (Jülich Aachen Research Alliance JARA).

## REFERENCES

- (1) Murakawa, H.; Onose, Y.; Miyahara, S.; Furukawa, N.; Tokura, Y. Comprehensive study of the ferroelectricity induced by the spin-dependent *d-p* hybridization mechanism in  $\text{Ba}_2\text{XGe}_2\text{O}_7$  ( $X = \text{Mn}, \text{Co}$ , and  $\text{Cu}$ ). *Phys. Rev. B: Condens. Matter Mater. Phys.* **2012**, *85*, 174106.
- (2) Hagiya, K.; Ohmasa, M.; Iishi, K. The modulated structure of synthetic Co-åkermanite,  $\text{Ca}_2\text{CoSi}_2\text{O}_7$ . *Acta Crystallogr., Sect. B: Struct. Sci.* **1993**, *49*, 172–179.
- (3) Hagiya, K.; Kusaka, K.; Ohmasa, M.; Iishi, K. Commensurate structure of  $\text{Ca}_2\text{CoSi}_2\text{O}_7$ , a new twinned orthorhombic structure. *Acta Crystallogr., Sect. B: Struct. Sci.* **2001**, *57*, 271–277.
- (4) Jia, Z. H.; Schaper, A. K.; Massa, W.; Treutmann, W.; Rager, H. Structure and phase transitions in  $\text{Ca}_2\text{CoSi}_2\text{O}_7$ - $\text{Ca}_2\text{ZnSi}_2\text{O}_7$  solid-solution crystals. *Acta Crystallogr., Sect. B: Struct. Sci.* **2006**, *62*, 547–555.
- (5) Kusaka, K.; Hagiya, K.; Ohmasa, M.; Okano, Y.; Mukai, M.; Iishi, K.; Haga, N. Determination of structures of  $\text{Ca}_2\text{CoSi}_2\text{O}_7$ ,  $\text{Ca}_2\text{MgSi}_2\text{O}_7$ , and  $\text{Ca}_2(\text{Mg}_{0.55}\text{Fe}_{0.45})\text{Si}_2\text{O}_7$  in incommensurate and normal phases and observation of diffuse streaks at high temperature. *Phys. Chem. Miner.* **2001**, *28*, 150–166.
- (6) Riestler, M.; Böhm, H. Phase transitions of modulated Co-åkermanite,  $\text{Ca}_2\text{CoSi}_2\text{O}_7$ . *Z. Kristallogr.* **1997**, *212*, 506–509.
- (7) Sazonov, A.; Hutanu, V.; Meven, M.; Roth, G.; Kézsmárki, I.; Murakawa, H.; Tokura, Y.; Náfrádi, B. The low-temperature crystal structure of the multiferroic melilite  $\text{Ca}_2\text{CoSi}_2\text{O}_7$ . *Acta Crystallogr., Sect. B: Struct. Sci., Cryst. Eng. Mater.* **2016**, *72*, 126–132.
- (8) Riestler, M.; Böhm, H.; Petricek, V. The commensurately modulated structure of the lock-in phase of synthetic Co-åkermanite,  $\text{Ca}_2\text{CoSi}_2\text{O}_7$ . *Z. Kristallogr. - Cryst. Mater.* **2000**, *215*, 102–109.
- (9) Barone, P.; Yamauchi, K.; Picozzi, S. Jahn-Teller distortions as a novel source of multiferroicity. *Phys. Rev. B: Condens. Matter Mater. Phys.* **2015**, *92*, 014116.
- (10) Hutanu, V.; Sazonov, A.; Murakawa, H.; Tokura, Y.; Náfrádi, B.; Chernyshov, D. Symmetry and structure of multiferroic  $\text{Ba}_2\text{CoGe}_2\text{O}_7$ . *Phys. Rev. B: Condens. Matter Mater. Phys.* **2011**, *84*, 212101.
- (11) Tovar, M.; Dinnebier, R. E.; Eysel, W. The  $\text{Cu}(\text{II})\text{O}_4$  Tetrahedron in the Åkermanite Structure. *Mater. Sci. Forum* **1998**, *278–281*, 750–755.
- (12) Mühlbauer, S.; Gvasaliya, S. N.; Pomjakushina, E.; Zheludev, A. Double-*k* phase of the Dzyaloshinskii-Moriya helimagnet  $\text{Ba}_2\text{CuGe}_2\text{O}_7$ . *Phys. Rev. B: Condens. Matter Mater. Phys.* **2011**, *84*, 180406.
- (13) Hutanu, V.; Sazonov, A. P.; Meven, M.; Roth, G.; Gukasov, A.; Murakawa, H.; Tokura, Y.; Szaller, D.; Bordács, S.; Kézsmárki, I.; Guduru, V. K.; Peters, L. C. J. M.; Zeitler, U.; Romhányi, J.; Náfrádi, B. Evolution of two-dimensional antiferromagnetism with temperature and magnetic field in multiferroic  $\text{Ba}_2\text{CoGe}_2\text{O}_7$ . *Phys. Rev. B: Condens. Matter Mater. Phys.* **2014**, *89*, 064403.
- (14) Masuda, T.; Kitaoka, S.; Takamizawa, S.; Metoki, N.; Kaneko, K.; Rule, K. C.; Kiefer, K.; Manaka, H.; Nojiri, H. Instability of magnons in two-dimensional antiferromagnets at high magnetic fields. *Phys. Rev. B: Condens. Matter Mater. Phys.* **2010**, *81*, 100402.
- (15) Perez-Mato, J. M.; Ribeiro, J. L. On the symmetry and the signature of atomic mechanisms in multiferroics: the example of  $\text{Ba}_2\text{CoGe}_2\text{O}_7$ . *Acta Crystallogr., Sect. A: Found. Crystallogr.* **2011**, *67*, 264–268.
- (16) Sazonov, A.; Meven, M.; Roth, G.; Georgii, R.; Kézsmárki, I.; Kocsis, V.; Tokunaga, Y.; Taguchi, Y.; Tokura, Y.; Hutanu, V. Origin of forbidden reflections in multiferroic  $\text{Ba}_2\text{CoGe}_2\text{O}_7$  by neutron diffraction: symmetry lowering or Renninger effect? *J. Appl. Crystallogr.* **2016**, *49*, 556–560.
- (17) Renninger, M. „Umweganregung“, eine bisher unbeachtete Wechselwirkungserscheinung bei Raumgitterinterferenzen. *Eur. Phys. J. A* **1937**, *106*, 141–176.
- (18) Rossmanith, E. Multiple diffraction in the kinematical approach. *Acta Crystallogr., Sect. A: Found. Crystallogr.* **2006**, *62*, 174–177.
- (19) Meven, M.; Sazonov, A. HEiDi: Single crystal diffractometer at hot source. *J. Large-scale Res. Facilities* **2015**, *1*, A7.
- (20) Georgii, R.; Seemann, K. MIRA: Dual wavelength band instrument. *J. Large-scale Res. Facilities* **2015**, *1*, A3.
- (21) Georgii, R.; Weber, T.; Brandl, G.; Skoulatos, M.; Janoschek, M.; Mühlbauer, S.; Pfeleiderer, C.; Böni, P. Position-sensitive detector system OBI for high resolution X-ray powder diffraction using on-site readable image plates. *Nucl. Instrum. Methods Phys. Res., Sect. A* **2018**, *881*, 60–64.
- (22) Sazonov, A. P. *Davinci: Software for visualization and processing of single-crystal diffraction data measured with a point detector*. <http://davinci.sazonov.org>.
- (23) Rossmanith, E. UMWEG: a program for the calculation and graphical representation of multiple-diffraction patterns. *J. Appl. Crystallogr.* **2003**, *36*, 1467–1474.
- (24) Petříček, V.; Dušek, M.; Palatinus, L. Crystallographic Computing System JANA2006: General features. *Z. Kristallogr. - Cryst. Mater.* **2014**, *229*, 345–352.
- (25) Becker, P. J.; Coppens, P. Extinction within the limit of validity of the Darwin transfer equations. I. General formalism for primary and secondary extinction and their applications to spherical crystals. *Acta Crystallogr., Sect. A: Cryst. Phys., Diffr., Theor. Gen. Crystallogr.* **1974**, *30*, 129–147.
- (26) Hutanu, V.; Sazonov, A.; Meven, M.; Murakawa, H.; Tokura, Y.; Bordács, S.; Kézsmárki, I.; Náfrádi, B. Determination of the magnetic order and the crystal symmetry in the multiferroic ground state of  $\text{Ba}_2\text{CoGe}_2\text{O}_7$ . *Phys. Rev. B: Condens. Matter Mater. Phys.* **2012**, *86*, 104401.
- (27) Shannon, R. D. Revised effective ionic radii and systematic studies of interatomic distances in halides and chalcogenides. *Acta Crystallogr., Sect. A: Cryst. Phys., Diffr., Theor. Gen. Crystallogr.* **1976**, *32*, 751–767.

## NOTE ADDED AFTER ASAP PUBLICATION

This paper was published on the Web on April 9, 2018, before the author text corrections were implemented. The corrected version was reposted on April 10, 2018.